# Nanoscale Block Copolymer Ordering Induced by Visible Interferometric Micropatterning: A Route towards Large Scale Block Copolymer 2D Crystals

Karim Aissou, Jonah Shaver, Guillaume Fleury, Gilles Pécastaings, Cyril Brochon, Christophe Navarro, Stéphane Grauby, Jean-Michel Rampnoux, Stefan Dilhaire, Georges Hadziioannou

# Nanoscale Block Copolymer Ordering Induced by Visible Interferometric Micropatterning: A Route towards Large Scale Block Copolymer 2D Crystals

*Karim Aissou, Jonah Shaver, Guillaume Fleury,* Gilles Pécastaings, Cyril Brochon, Christophe Navarro, Stéphane Grauby, Jean-Michel Rampnoux, Stefan Dilhaire,* and Georges Hadziioannou**

Perfectly ordered microstructures with nanometrically defined periodicity offer promising opportunities in microelectronic applications and nanotechnologies for the production of high-density magnetic storage media, plasmonic-based devices, and advanced CMOS digital circuits. To produce long-range ordered two-dimensional arrays inherent to such technologies, the hybrid combination of "bottom-up" self-assembly and "top-down" guiding patterned templates has been successfully introduced. This has led to new technological breakthroughs wherein the self-assembly of block copolymers (BCPs) are the cornerstone of the "bottom-up" nanofabrication processes through their segregation behavior into periodic mesostructures.[1–6] Well-ordered 2D arrays of block copolymers are produced by solvent or thermal annealing thin films cast onto grooved substrates when the block copolymer equilibrium period is commensurate with the dimension of the guiding template.[4] However, as the understanding of "bottom up"-type approaches is constantly improving, progress with "top-down"-type techniques is stagnating, since they have been already quite well developed and understood for many years. Methods used to fabricate topographic surface patterns over large areas with nanometric precision present some technological limitations. For example, electron-beam (e-beam) lithography is a slow, serial, lithographic process. More recently, surface reconstruction upon heating of mis-cut single-crystal sapphire wafers has been successfully used to generate highly-ordered and ultradense arrays of block copolymer thin films in spite of some residual topological defects and of a distribution of pitches over the surface topography.[6] Even if sapphire wafers are not the standard substrate in the microelectronic industry, this "faceted substrate" methodology, theoretically envisioned by Joanny et al.,[7] has paved the way in order to overcome the problem of commensurability between the field pattern and the BCP domain lattice encountered with graphoepitaxial confinement.

Here we describe a novel topographical methodology to control the self-assembly of block copolymers into highly-ordered 2D arrays through a guiding pattern created from a multifunctional copolymer sub-layer which combines cooperative motion of azo-chromophores, with purposely added cross-linkable pendant groups along the polymer backbone. The generation of topography is related to the trans-cis photo-isomerization of the diazoic bonds leading to a surface-relief grating[8] in the multifunctional copolymer sub-layer, subsequently frozen by crosslinking. This association of functionalities on a random copolymer can be used to produce highly-ordered 2D arrays. This route does not suffer from many of the inconveniences encountered in the aforementioned methodologies. It permits fast, low cost fabrication of defect-free sinusoidal patterns with controllable pitches and amplitudes on arbitrary substrates such as silicon wafers or polymeric flexible substrates. A direct application derived from such highly-ordered 2D arrays is their use as guide to drive the self-assembly of functional (magnetic, light-emitting…) nano-objects such as nanoparticles and nanorods via a nanocomposite thin film approach.[9–11]

For block copolymer thin films spanning across the edges of the topological patterns, domain localization is mainly dictated by the overall lateral ordering while the substrate topography controls the directional orientation of the block copolymer array. Indeed a lower entropic penalty is induced by this behavior as compared to that which exactly follows the substrate topography.[6] Consequently, the key to pattern block copolymer domains into highly-ordered 2D arrays is the definition of the optimal conditions allowing for efficient healing through the lateral assembly of the defects arising from the substrate topography. To illustrate this phenomenon, we have studied the effect of the block copolymer surface deformation magnitude on defect annihilation mechanisms in order to obtain highly ordered 2D arrays of block copolymer nanodomains on azobenzene containing topological patterns.

**Figure 1** illustrates the different processing steps used to prepare the highly-ordered 2D arrays on the surface-relief grating pattern. **Figure 2**a presents a 3D-AFM topographic image obtained from a surface-relief pattern inscribed into a 200 nm thick azobenzene containing polymer layer. A pitch of 375 nm

Dr. K. Aissou, Dr. G. Fleury, Dr. G. Pecastaings,
Dr. C. Brochon, Prof. G. Hadziioannou
Laboratoire de Chimie des Polymères Organiques
Univ. Bordeaux
CNRS, LCPO, UMR 5629, F-33600 Pessac, France
E-mail: gfleury@enscbp.fr; hadzii@enscbp.fr
Dr. J. Shaver, Dr. S. Grauby,
Dr. J.-M. Rampnoux, Pr. S. Dilhaire
Laboratoire Ondes et Matière d'Aquitaine
Univ. Bordeaux
CNRS, LOMA, UMR 5798, F-33400 Talence, France
E-mail: stefan.dilhaire@u-bordeaux1.fr
Dr. C. Navarro
ARKEMA, Groupement de Recherches de Lacq
RN 117, BP 34, F-64170 Lacq Cedex, France

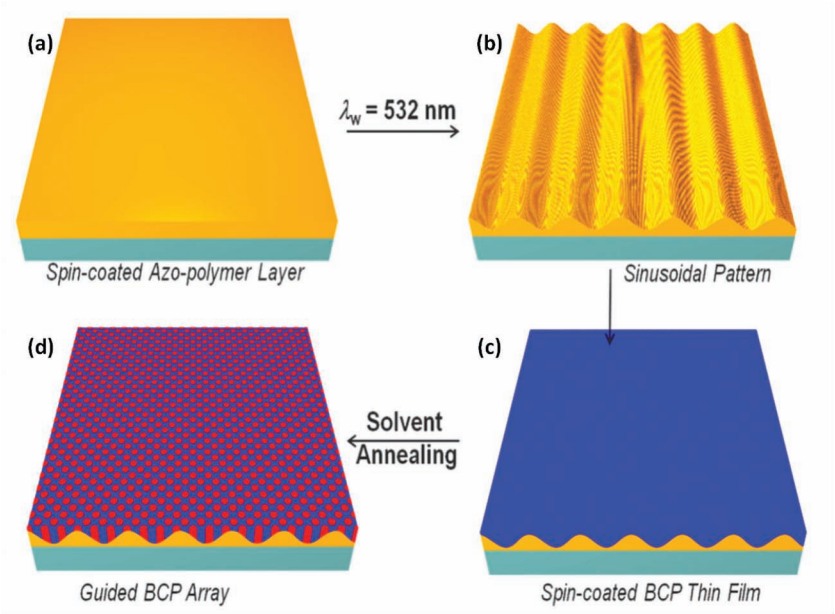


**Figure 1.** Schematic process flow to generate highly-ordered 2D array of block copolymer thin film on a sinusoidal pattern: (a) azobenzene containing copolymer chains deposition, (b) sinusoidal pattern inscription onto the azobenzene containing copolymer layer using a $\lambda_w = 532$ nm writing laser wavelength (c) irradiation of the sinusoidal pattern under a red light laser source ($\lambda_f = 686$ nm) to freeze the structure followed by the block copolymer thin film deposition, and (d) formation of highly-ordered cylindrical domains in the block copolymer layer after a solvent annealing treatment.

and an amplitude of 10 nm was extracted from the height cross section profile (see Figure S4a). The amplitude was adjusted by varying the exposure time of the azobenzene containing layer under the laser beam (see also Figure S3) leading to surface-relief grating producing a typical sinusoidal pattern defined by the dimensionless parameter, $(aq)_{pattern}$, where $a$ and $q$ ($q = 2\pi/\Lambda$) are the pattern amplitude and wavenumber, respectively. Figure 2b shows a 3D-AFM topographic image of PS-*b*-PEO thin film spin-coated from a benzene solution onto the sinusoidal pattern presented in Figure 2a. After a solvent-annealing treatment in a benzene/water vapor environment,[11] the PS-*b*-PEO thin film having an average film thickness, $t \sim 50$ nm, exhibited a hexagonal close-packed (HCP) structure with an inter-domain spacing, $d$, of 28.6 nm extracted from the 2D-FFT intensity profile (see Figure S4c). Moreover, the height cross-section profile indicates that the PS-*b*-PEO film free surface presents a periodic structure characterized by a pitch of $\Lambda = 375$ nm and an amplitude of ~ 1 nm (see Figure S4b).

Recent theoretical work[12,13] has shown that curving a hexagonal lattice above a critical value introduces stresses that can be relieved by the introduction of defects. For a sine wave patterned surface, the dimensionless parameter, $(aq)$, describes the surface deformation magnitude. Above the critical magnitude $(aq)_c$, a defect-free hexagonal lattice becomes unstable and defects appear in the lattice, which relieves stresses caused by the geometrical constraints. In order to determine how the surface deformation magnitude $(aq)$ affects the defect density in the 2D lattice, PS-*b*-PEO layers with different film thicknesses were studied using Delaunay triangulation constructions for the recognition and the localization of defect sites. To maintain the confinement of the 2D-array of cylindrical nanodomains while reducing the undesirable stresses of the lattice imposed on the PS-*b*-PEO film free surface, the BCP layer thickness was progressively increased until reaching the critical magnitude of the free surface, $(aq)_{PS\text{-}b\text{-}PEO}$, for which a defect-free hexagonal lattice becomes stable. For an amplitude of 1 nm, the modulated PS-*b*-PEO film ($t \sim 50$ nm) is composed of well-organized areas (grains), corresponding to regions where all cylinders are 6-fold coordinated (see **Figure 3**a). These areas are separated by topological defects known as dislocations and disclinations.[14,15] Under such conditions, the surface-relief grating influences the directional orientation of the PEO nanodomains. Indeed, grains with anisotropic shape (i.e. elongated in the direction of the substrate pattern) are distributed with low angle grain boundaries (LAGBs) over the surface, as shown in Figure S8. This is in contrast to those observed in a microphase-separated PS-*b*-PEO thin film deposited on a non-patterned substrate.[11] However, some dislocation lines cross several valleys of the underlying surface-relief pattern indicating that the influence of the topographical substrate is limited. These results are emphasized by the corresponding 2D-FFT that shows 6-fold angular symmetry with azimuthally broadened spots (i.e. characteristic to a hexagonal array not in a 2D-crystal phase) superimposed on the two low frequency spots of the sinusoidal pattern. To quantify the 2D-order of the PS-*b*-PEO film, the bond-orientational correlation function, $G_6(r)$, (see Figure S5) and the pair-correlation function, $g(r)$, (see Figure S6) have been plotted following the method proposed by Quinn et al.[16] (see Supporting Information for details). Both exponential ($\sim\exp[-r/\xi_6]$) and power decay ($\sim r^{-\eta}$) functions have been used to fit the $G_6(r)$ data. An orientational correlation length, $\xi_6 = (495 \pm 83)\ d$, and a power exponent, $\eta = (0.082 \pm 0.005)$, were extracted from these fits, indicating a quasi long-range orientational order. The envelope of $g(r)$ was fitted by an exponential decay ($\sim\exp[-r/\xi_T]$) where the translational correlation length, $\xi_T$, was found to be equal to $(17 \pm 2)\ d$. As $\xi_T < \xi_6$ and $\eta < 0.25$, we conclude that the microstructure is quenched in a hexatic phase as predicted by the Kosterlitz–Thouless-Halperin-Nelson-Young (KTHNY) theory. Figure 3b shows a 3D-AFM topographic image obtained from a thicker PS-*b*-PEO film ($t \sim 65$ nm) with a 0.5 nm surface amplitude. The Delaunay triangulation reveals a hexatic intermediate phase of the 2D array of cylinders[17] with only few dislocations (5–7 coordinated cylinders) preferentially located near the highest points on the free surface. Here, the 2D-FFT exhibits six sharper first-order spots concurrent with both an increase of the translational correlation length ($\xi_T = (20 \pm 1)\ d$) and the quasi long-range orientational order ($\eta = 0.059 \pm 0.003$)) (see Figure S5 and S6). The anchoring of dislocations close to height-maxima is caused by lattice stresses induced by the patterned substrate

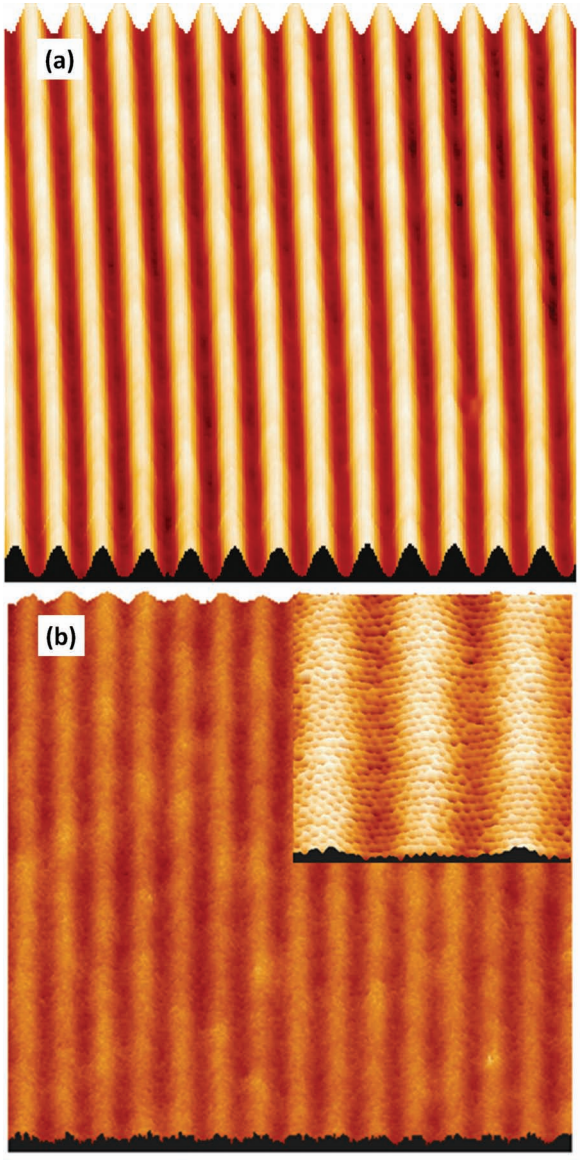


**Figure 2.** (a) (5 × 5 μm) 3D-AFM topographic views obtained from a sinusoidal pattern, inscribed onto the azobenzene-based layer, with a pitch and amplitude of about 375 nm and 10 nm, respectively, and (b) after deposited and solvent annealed PS-*b*-PEO layer. The film free surface presents an amplitude of about 1 nm. Inset: (1 × 1 μm) magnified 3D-AFM topographic view showing that the PS-*b*-PEO film exhibits a hexagonal close-packed cylinder structure.

which acts as a uniform external field controlling the equilibrium position of the dislocations.[12] Vitelli et al. found that the dislocations can not easily diffuse due to the suppression of the glide process which is the dominant form of motion at low temperature.[13] Thus, the geometrical constraints, anchoring the dislocations close to the top of the wave and impinging their ability to diffuse, freeze the film in a hexatic intermediate phase since the defect healing processes, such as annihilation of two separate 5–7 pairs, are suppressed.[18,19] By increasing the average film thickness to a critical value, $t_c \sim 65$ nm, where the top of the PS-*b*-PEO layer presents a smooth free-surface with no hint of the underlying sinusoidal pattern, a defect-free area (single grain) is formed over a large surface (see Figure 3c). In the 2D-FFT inset we observe the extinction of the two low frequency peaks of the underlying sinusoidal pattern. In addition, the HCP peaks become much sharper, and higher orders appear. Both are the signature of a 2D-crystal order confirmed by the long-range orientational order of the microstructure ($G_6(r)$ = constant) and the $g(r)$ function profile which exhibits oscillations clearly visible over 25 $d$ with an algebraic decay of its envelope ($\sim r^{-\eta_T}$ where $\eta_T = (0.165 \pm 0.021)$) (see Figure S6). These results shows that the long-range order of the 2D-array is strongly affected by the stresses (induced by the topographical pattern) of the PS-*b*-PEO film which play a crucial role on the diffusion of defects, and hence, on their annihilation. Indeed, for a flat polymer free surface the glide dynamics of isolated dislocations is not constrained since only small energy barriers are present corresponding to a periodic Peierls potential.[20] If the film is made thicker than $t_c$, however, the long-range order of the cylindrical nanodomains is lost. This indicates a decorrelation between the surface-relief grating substrate and the lateral orientation of the hexagonally packed PEO cylinders (see Figure S7). In very thick films, the influence of the substrate on the lateral hexagonal close packing of PEO cylinders becomes negligible. Hence, we conclude that there is an optimum PS-*b*-PEO film thickness at which the sinusoidal pattern will form large defect-free grain. **Figure 4** shows an AFM phase image (2 × 2 μm), which enhances the contrast between the domains of a solvent-annealed PS-*b*-PEO layer, with a thickness close to the optimal value. This film exhibits a nearly defect free single grain. The 2D-FFT shows multiple sharp higher-order peaks characteristic of a long-range ordering of the PEO cylindrical nanodomain array formed on the sinusoidal grating pattern. This demonstrates that our approach opens a versatile route to generating dense, highly-ordered two-dimensional block copolymer thin film arrays on various substrates.

We have demonstrated a very simple and low-cost route to fabricate highly-ordered and dense arrays of block copolymer thin films on silicon substrates using sinusoidal surface-relief gratings interferometrically inscribed onto an azobenzene containing layer with a visible laser beam. High quality sinusoidally modulated patterns, formed over wafer-scale areas in minutes, will provide an excellent platform to guide block copolymer self-assembly. To favor the formation of a block copolymer layer with large defect-free areas, we have shown that an optimum film thickness is required. This optimally average thick layer ($t_c \sim 65$ nm) corresponds to the critical film thickness for which the block copolymer thin film presents a smooth free surface with no hint of the underlying surface-relief pattern, i.e. a depth that completely fills the underlying pattern. In addition, it is noteworthy that the tailoring of the BCP film thickness may be needed for some applications. This issue could be overcome by matching the amplitude of the surface relief grating topography to the critical value ensuring the confinement effect needed for a particular BCP film thickness in order to produce highly ordered BCP 2D arrays. The use of this methodology to generate lithographic masks could be envisioned by using BCPs designed with a non-sacrificial

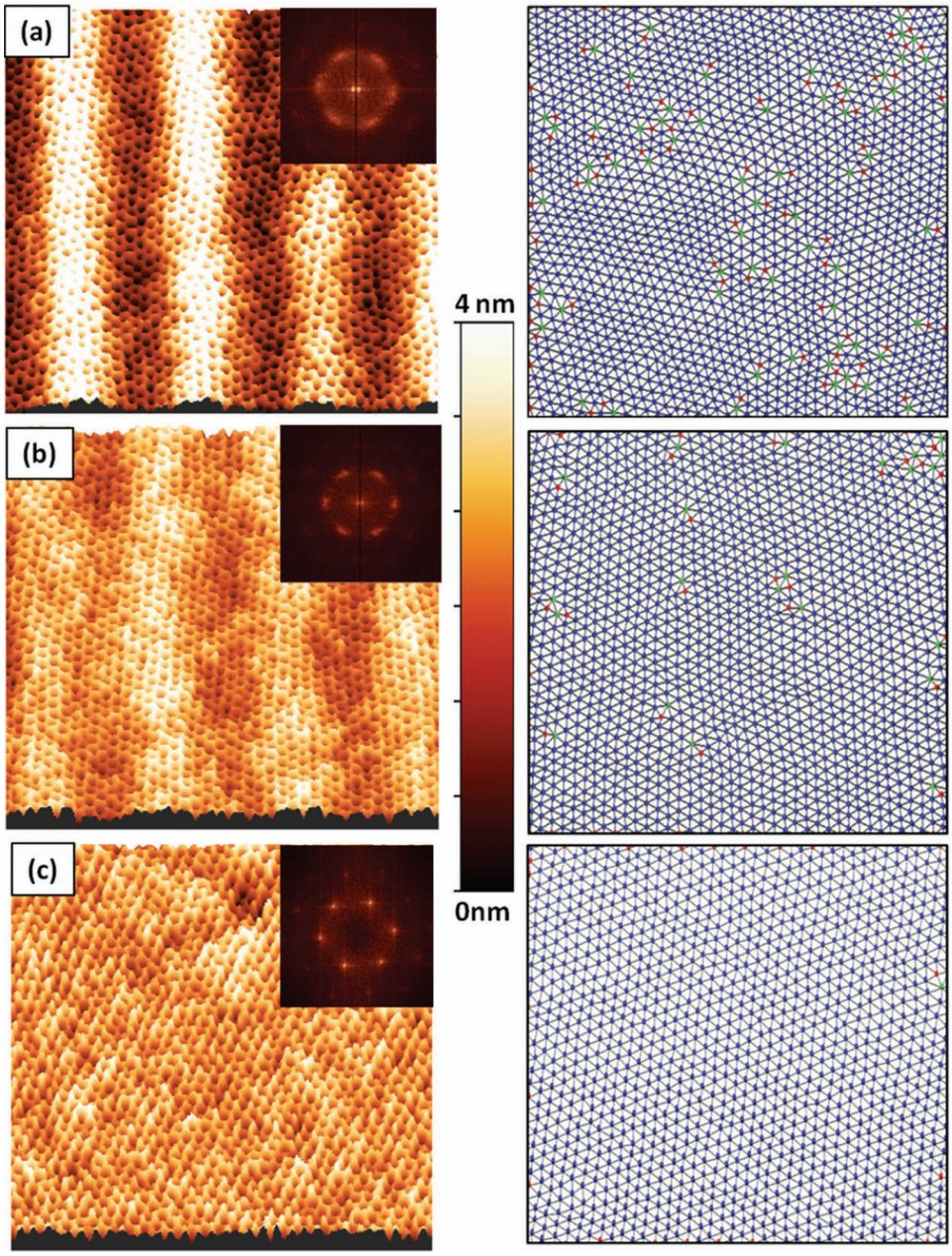


**Figure 3.** 3D visualizations of the AFM height images showing microphase-separated PS-*b*-PEO thin films spin-coated on a sinusoidal pattern, which have different film thicknesses (left column) along with their associated Delaunay triangulations (right column) and Fourier transforms (insets). (1.25 × 1.25 μm). (a): When the film free surface presents an amplitude of ~ 1 nm, the Delaunay triangulation shows organized grains which correspond to regions where all PEO spheres are 6-fold coordinated (blue dots). These grains are delimited by 7-fold (green dots) and 5-fold (red dots) coordinated cylinders. The 2D-FFT shows six distinct broad first-order Bragg peaks, indicating the presence of defects superimposed to the two low frequency peaks of the sinusoidal pattern. (b): For an amplitude of ~0.5 nm, the Delaunay triangulation reveals a single grain orientation and few dislocations preferentially located near the height-maximums on the free surface. The first-order peaks in the 2D-FFT appear slightly sharper as the system is now into a hexatic phase whereas the two low frequency peaks are still observed. (c): For the PS-*b*-PEO layer presenting a free surface with no hint of the underlying sinusoidal pattern, the Delaunay triangulation reveals the film is defect-free over the scan area. The 2D-FFT showing six sharp first-order peaks as well as sharp second and third-order peaks visible in this Fourier transform further indicate the presence of a single, well-formed hexagonal grain.

block exhibiting a high etch resistivity in regard to the azobenzene containing sub-layer. Block copolymers containing siloxane-type units could be promising candidates and work to demonstrate the feasibility of such an approach is currently in progress.

## Experimental Section

*Materials and Methods*: A 200 nm layer of azobenzene containing copolymers designed with cross-linkable pendant functionalities along the polymer backbone (see Supporting Information for details) were first deposited on a silicon substrate. Then, the photo-induced motion

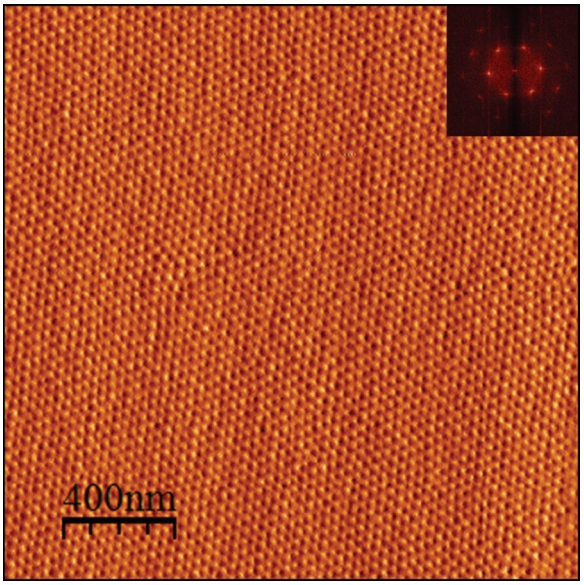


**Figure 4.** AFM phase image of a solvent annealed film with highly ordered PEO cylindrical microdomains (2 × 2 µm). Inset: 2D-FFT showing multiple higher-order interferences characteristic of the long-range ordering of the cylindrical nanodomain array.

property of azobenzene groups was exploited to inscribe sinusoidal patterns through surface-relief grating in the polymer film using a Lloyd's mirror interferometer set up (Figure S1).[8,21] A *p*-polarized laser beam ($\lambda_w$ = 532 nm) with a fluence of 30 mW cm$^{-2}$ was split into two beams, one directly incident onto the film and the other reflected by a mirror to which the film was perpendicularly attached. A large range of pitches, $\Lambda = \lambda_w/2\sin\theta$ (where $\theta$ is the incident angle of the writing beams onto the substrate), were obtained by rotating the sample holder/mirror with respect to the incident beam (see also Figure S2). For this step, the writing laser wavelength, $\lambda_w$, was selected to match the absorption band of the azobenzene chromophores in order to induce the trans-cis photoisomerization responsible for the surface-relief grating.[8] To freeze the sinusoidal patterns, a red laser source ($\lambda_f$ = 686 nm) cross-linked the azobenzene containing copolymer film swelled with additional trifunctional acrylate monomers through the use of an infrared photoinitiator having an absorbance range from 575 to 700 nm. Finally, a poly(styrene-*block*-ethylene oxide) (PS-*b*-PEO) ($M_n$ = 43 kg/mol, $\Phi_{PEO}$ = 0.25) block copolymer thin film was spin-coated on the resulting sinusoidal pattern which served to guide the formation of highly-ordered cylindrical PEO domains perpendicularly oriented to the substrate during the subsequent solvent annealing process. The solvent annealing process leading to cylindrical PEO domains perpendicularly oriented to the substrate is the same for all the films and follows the procedure already reported in details in our previous work.[11]

## Acknowledgements

The authors are grateful to Arkema, the Région Aquitaine and the French National Agency for Research (ANR-09-NANO-026-01) for financial support of this work.

[1] R. A. Segalman, H. Yokoyama, E. J. Kramer, *Adv. Mater.* **2001**, *13*, 1152–1156.
[2] J. Y. Cheng, C. A. Ross, E. L. Thomas, H. I. Smith, G. J. Vancso, *Appl. Phys. Lett.* **2002**, *81*, 3657–3659.
[3] J. Y. Cheng, C. A. Ross, E. L. Thomas, H. I. Smith, G. J. Vancso, *Adv. Mater.* **2003**, *15*, 1599–1602.
[4] J. Y. Cheng, A. M. Mayes, C. A. Ross, *Nat. Mater.* **2004**, *3*, 823–828.
[5] H.-W. Li, W. T. S. Huck, *Nano Lett.* **2004**, *4*, 1633–1636.
[6] S. Park, D. H. Lee, J. Xu, B. Kim, S. W. Hong, U. Jeong, T. Xu, T. P. Russell, *Science* **2009**, *323*, 1030–1033.
[7] M. S. Turner, J. F. Joanny, *Macromolecules* **1992**, *25*, 6681–6689.
[8] T. Ubukata, T. Isoshima, M. Hara, *Adv. Mater.* **2005**, *17*, 1630–1633.
[9] S. B. Darling, N. A. Yufa, A. L. Cisse, S. D. Bader, S. J. Sibener, *Adv. Mater.* **2005**, *17*, 2446–2450.
[10] A. Haryono, W. H. Binder, *Small* **2006**, *2*, 600–611.
[11] K. Aissou, G. Fleury, G. Pecastaings, T. Alnasser, S. Mornet, G. Goglio, G. Hadziioannou, *Langmuir* **2011**, *27*, 14481–14488.
[12] A. Hexemer, V. Vitelli, E. J. Kramer, G. H. Fredrickson, *Phys. Rev. Lett. E* **2007**, *76*, 051604–12.
[13] V. Vitelli, J. B. Lucks, D. R. Nelson, *Proc. Natl. Acad. Sci. USA* **2006**, *103*, 12323–12328.
[14] R. A. Segalman, A. Hexemer, R. C. Hayward, E. J. Kramer, *Macromolecules* **2003**, *36*, 3272–3288.
[15] K. Aissou, T. Baron, M. Kogelschatz, A. Pascale, *Macromolecules* **2007**, *40*, 5054–5059.
[16] R. A. Quinn, C. Cui, J. Goree, J. B. Pieper, H. Thomas, G. E. Morfill, *Phys. Rev. E* **1996**, *53*, R2049–R2052.
[17] The continuous melting transition from a 2D crystal to a liquid proceeds through a hexatic intermediate phase. See the following reference for further details: R. A. Segalman, A. Hexemer, E. J. Kramer, *Macromolecules* **2003**, *36*, 6831–6839.
[18] C. Harrison, D. E. Angelescu, M. Trawick, Z. Cheng, D. A. Huse, P. M. Chaikin, D. A. Vega, J. M. Sebastian, R. A. Register, D. H. Adamson, *Europhys. Lett.* **2004**, *65*, 800–806.
[19] D. E. Angelescu, J. H. Waller, D. H. Adamson, P. Deshpande, S. Y. Chou, R. A. Register, P. M. Chaikin, *Adv. Mater.* **2004**, *16*, 1736–1740.
[20] A. D. Pezzutti, D. A. Vega, M. A. Villar, *Phil. Trans. R. Soc. A* **2011**, *369*, 335–350.
[21] A. Natansohn, P. Rochon, *Chem. Rev.* **2002**, *102*, 4139–4176.